nature structural & molecular biology

A conformational switch in PRP8 mediates metal ion coordination that promotes pre-mRNA exon ligation

Matthew J Schellenberg[1,4,5], Tao Wu[1,5], Dustin B Ritchie[1,4], Sebastian Fica[2], Jonathan P Staley[2], Karim A Atta[1], Paul LaPointe[3] & Andrew M MacMillan[1]

Splicing of pre-mRNAs in eukaryotes is catalyzed by the spliceosome, a large RNA-protein metalloenzyme. The catalytic center of the spliceosome involves a structure comprising the U2 and U6 snRNAs and includes a metal bound by U6 snRNA. The precise architecture of the splicesome active site, however, and the question of whether it includes protein components, remains unresolved. A wealth of evidence places the protein PRP8 at the heart of the spliceosome through assembly and catalysis. Here we provide evidence that the RNase H domain of PRP8 undergoes a conformational switch between the two steps of splicing, rationalizing yeast *prp8* alleles that promote either the first or second step. We also show that this switch unmasks a metal-binding site involved in the second step. Together, these data establish that PRP8 is a metalloprotein that promotes exon ligation within the spliceosome.

The spliceosome is a large RNP particle consisting of the U1, U2 and U4–U5–U6 small nuclear ribonucleoprotein particles (snRNPs), with each containing a unique snRNA and associated proteins bound to the pre-mRNA substrate[1–3]. Spliceosome assembly is a complex process that includes formation of a U2–U6 snRNA structure that has been shown to be essential for catalysis of splicing transesterifications[4]. Although pre-mRNA splicing is therefore believed to be intrinsically RNA catalyzed, there is considerable evidence suggesting an intimate interaction between spliceosomal proteins and the active site of the spliceosome. The highly conserved U5 snRNP protein PRP8 has been shown in a cross-linking study to directly contact the 5′ splice site and U6 snRNA during spliceosome assembly[5–7]. Mutant *prp8* alleles in yeast also suggest interactions of this factor with both substrate and snRNA catalytic structures in the spliceosome[8–12]. Therefore, the catalytic center of the spliceosome may include protein as well as RNA components[13].

A large number of mutant *prp8* alleles related to spliceosome activation and possibly catalysis have been characterized in yeast, which suggests a central role for this factor in both processes, including a proposed conformational change between the two steps of splicing[8,12]. The clustering of these alleles, along with cross-linking data, suggested the presence of a core domain within PRP8 that could be part of or interact with the spliceosomal catalytic machinery[12,13]. To test these hypotheses, we examined the role of this domain of PRP8 within the spliceosome by using a combination of X-ray structure determination and characterization of mutant *prp8* alleles in yeast and yeast splicing extracts.

RESULTS

PRP8 rearrangement unmasks a conserved metal-binding site

We and others recently solved the X-ray structures of the human and yeast domain IV of PRP8 (refs. 14–16; hereafter referred to as PRP8 RH). This domain is C terminal to reverse transcriptase–derived and endonuclease-like domains and N terminal to a Jab-MPN domain within PRP8 (ref. 17; **Supplementary Fig. 1a**,**b**). Here, we report our detailed structural analysis of PRP8 RH and a panel of domain mutants, highlighting a conformational change that unmasks a Mg^{2+}-binding site that promotes splicing (**Fig. 1**, **Table 1** and **Supplementary Tables 1** and **2**). Our previously described crystals of human PRP8 RH (amino acids (aa) 1769–1990) included two monomers in the asymmetric unit. A salient feature was the presence of an N-terminal RNase H domain that included a 17-aa insertion (aa 1787–1803) between two adjacent β-strands of the fold. Within the crystal, in what we describe as the closed conformation, this insertion forms a two-stranded antiparallel β-hairpin, whereas in the second, open conformation this hairpin is disrupted to form a displaced loop (**Supplementary Note 1**). The translation of this loop back by ~45° pulls aa 1782–1784 to extend the β1 strand of the RNase H fold (**Fig. 1a** and **Supplementary Movie 1**). This movement is related to the disruption and rearrangement of elements of the α1 helix and part of the α2 helix (aa 1823–1839). These residues now partially fill the space formerly occupied by the base of the hairpin.

The presence of an RNase H fold within a domain of PRP8 associated with the individual catalytic steps of splicing is notable because RNase H is a metalloenzyme promoting chemistry on an RNA

[1]Department of Biochemistry, University of Alberta, Edmonton, Alberta, Canada. [2]Department of Molecular Genetics and Cell Biology, University of Chicago, Chicago, Illinois, USA. [3]Department of Cell Biology, University of Alberta, Edmonton, Alberta, Canada. [4]Present addresses: Laboratory of Structural Biology, National Institute of Environmental Health Sciences, National Institutes of Health, US Department of Health and Human Services, Research Triangle Park, North Carolina, USA (M.J.S.) and Department of Physics, University of Alberta, Edmonton, Alberta, Canada (D.B.R.). [5]These authors contributed equally to this work. Correspondence should be addressed to A.M.M. (andrew.macmillan@ualberta.ca).

Received 29 January; accepted 12 March; published online 19 May 2013; doi:10.1038/nsmb.2556

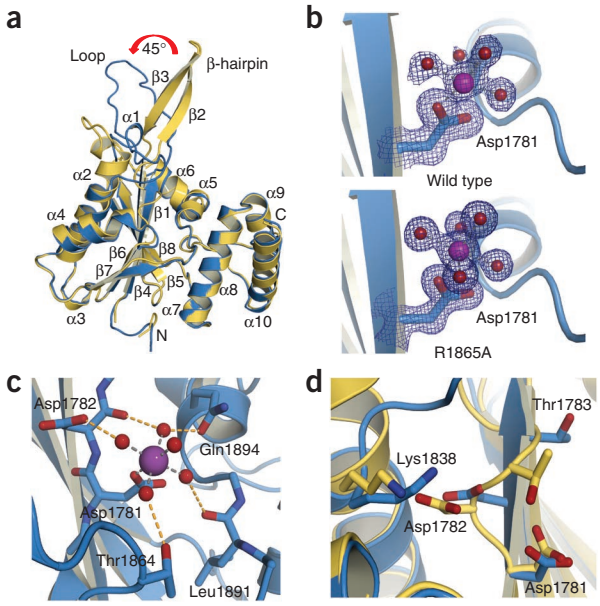

Figure 1 Conformational switch in the PRP8 RH domain unmasks a Mg^{2+}-binding site. (**a**) X-ray structure of the PRP8 RH domain. Superposition of the closed (yellow) and open (cyan) conformations observed in the asymmetric unit. (**b**) $2F_o - F_c$ maps contoured at 1.0σ showing octahedral coordination of Mg^{2+} (purple) bound in the open conformation of wild-type and R1865A PRP8 RH. (**c**) Detail of Mg^{2+}-ion (purple) coordination by Asp1781 and inner-sphere waters (red) in the open conformation of PRP8 RH. (**d**) Superposition of the X-ray structure of the PRP8 RH domain closed (yellow) and open (cyan) conformations, detailing the displacement of Thr1783 to allow Mg^{2+} coordination. The metal ion bound in the open conformation is not shown for clarity.

substrate. Catalysis of RNA cleavage by RNase H–like enzymes involves a two-metal mechanism in which divalent magnesium ions, bound at adjacent sites separated by ~4 Å, promote hydrolysis by activation of a water nucleophile combined with transition-state stabilization[18]. Thus, the presence of the RNase H domain in a portion of PRP8 associated with the spliceosomal catalytic core raised the possibility that a protein-bound metal could participate in catalysis of splicing. Inspection of the PRP8 RH structure[14–16] showed that one of two canonical RNase H metal-binding sites is present: two aspartates (Asp1781 and Asp1782) with coordinating side chains spatially conserved with respect to Mg^{2+}-coordinating residues within the RNase H fold. This site is completely conserved in all PRP8 orthologs (**Supplementary Fig. 1c**). In our initial studies, despite the presence of $MgCl_2$ during crystallization, we did not observe metal ion coordination at this site, a result that we attribute to the high ionic strength (2.5 M NaCl) of the crystallization conditions[14]. Additionally, the side chain of the conserved arginine residue Arg1865 positioned over this site possibly has a shielding role. In the work reported here, we crystallized and solved the 1.4-Å structure of PRP8 RH and the 1.15-Å structure of the R1865A mutant under low ionic strength but in the presence of divalent magnesium. Again, we observed both closed and open conformations of PRP8 RH in the asymmetric units of the crystals. However, under these conditions we noted coordination of a single magnesium ion at the conserved metal-binding site within the open, but not the closed, conformation of both wild-type and R1865A PRP8, confirming this observation by anomalous scattering from Co^{2+}-soaked crystals (**Fig. 1b**, **Supplementary Fig. 2a** and **Table 1**). The electron density suggests that the Mg^{2+} ion is present at partial occupancy in the wild-type structure but is consistent with full occupancy in the R1865A structure. The overall features of the R1865A crystals and the resulting structure are markedly similar to those of wild type. A higher metal occupancy is consistent with a shielding role of the arginine side chain in the wild-type protein, which we propose could be relieved by rearrangement associated with RNA binding within the spliceosome.

Coordination of a metal ion to the canonical RNase H site of PRP8 includes inner-sphere contact with the side chain of Asp1781 and outer-sphere coordination through five ordered waters to the carboxylate of Asp1782, the carbonyls of Asp1782 and Leu1891, the amide carbonyl of Gln1894 and the hydroxyl of Thr1864 (**Fig. 1c**). One consequence of the structural rearrangement involved in the closed-to-open transition is that Asp1782 moves closer to Asp1781 and Thr1783 is displaced by ~4 Å upward (**Fig. 1d** and **Supplementary Movie 1**). In the closed conformation, it is this positioning of Thr1783 that essentially blocks metal binding at this site; the substantial local reorganization of the PRP8 RH structure is essential to allow Mg^{2+} coordination. These observations led us to investigate the possible roles of both the conformational change and conformation-dependent Mg^{2+} coordination by PRP8 in the spliceosome.

prp8 suppressor alleles favor closed or open conformations

A previous study has suggested an elegant model whereby PRP8 is involved in the equilibrium between two distinct spliceosomal conformations associated with the first and second transesterification steps[19]. Two sets of *prp8* alleles, designated as first or second step, are proposed to act by shifting this equilibrium to favor one step over the other. Thus a first-step allele suppresses a defect in the first but enhances a defect in the second step of splicing, whereas a

Table 1 Data collection and refinement statistics

	WT, 300 mM $MgCl_2$	R1865A, 300 mM $MgCl_2$
Data collection[a]		
Space group	$P2_12_12_1$	$P2_12_12_1$
Cell dimensions		
a, *b*, *c* (Å)	76.03, 78.02, 93.81	76.20, 78.04, 94.06
Resolution (Å)	1.4	1.15
R_{sym}	0.069 (0.525)	0.038 (0.482)
$I / \sigma I$	18.1 (2.3)	26.7 (2.5)
Completeness (%)	99.5 (99.5)	98.9 (96.6)
Redundancy	4.9	4.3
Refinement		
Resolution (Å)	60–1.40	60–1.15
No. reflections	109,740	186,162
R_{work} / R_{free}	0.136 / 0.177	0.140 / 0.160
No. atoms		
Protein	3,757	3,884
Ligand/ion	19	26
Water	709	735
B factors		
Protein	21.5	23.4
Ligand/ion	28.2	27.4
Water	34.6	35.9
r.m.s. deviations		
Bond lengths (Å)	0.011	0.012
Bond angles (°)	1.44	1.51

Each data set was collected from a single crystal.
[a]Values in parentheses correspond to the highest-resolution shell (10% of reflections).
WT, wild type.

second-step allele suppresses a defect in the second but enhances a defect in the first step of splicing. Notably, the largest proportion of first- or second-step suppressor alleles associated with the PRP8 RH domain map to the two-stranded β-hairpin or rearranged loop[14–16] (**Supplementary Fig. 1d**). This suggests that the disposition of this structure is critical to the function of this domain within the spliceosome. Because of this, we endeavored to determine whether first- or second-step phenotypes associated with specific alleles could be rationalized by reference to either of the two conformations observed crystallographically.

We first generated mutant yeast strains to characterize the effect on splicing of a series of mutations within the PRP8 RH β-hairpin, comparing these to both wild-type and known strong first-step (E1960K) and second-step (V1870N; **Supplementary Fig. 1d** and **Supplementary Table 2**) alleles. We assayed growth by using a copper-resistance reporter system in which the branch-site A of the ACT1-CUP1 intron was replaced with G (BSG), a change that inhibits the second step of splicing[20]. Three mutant alleles (E1960K, V1860D and T1872E) caused less resistance to copper, consistent with a first-step phenotype, whereas three alleles (V1870N, T1861P and V1862Y) caused more resistance to copper, consistent with a second-step phenotype (**Fig. 2a**). We directly assayed steady-state pre-mRNA splicing efficiencies of the reporter gene in these mutant PRP8 backgrounds, comparing splicing of the BSG mutant ACT1-CUP1 intron with an RNA containing the branch-site C mutation (BSC), known to inhibit both steps of splicing[21]. Consistent with the results of the growth assay, E1960K, V1860D and T1872E acted as first-step alleles, enhancing the first step of splicing in the presence of BSC at the expense of the second step and worsening the effect of the BSG mutation. Conversely, V1870N, T1861P and V1862Y acted as second-step alleles, enhancing the second step in splicing of the BSG introns (**Fig. 2b** and **Supplementary Note 2**).

We next crystallized and solved the X-ray structures of four human PRP8 RH mutants corresponding to the yeast alleles mapping to the β-hairpin under conditions such that the asymmetric unit featured both the closed and open conformations (**Fig. 3a**,**b**, **Supplementary Fig. 3a**,**b** and **Supplementary Table 1**). In all cases, a bound metal ion was observed at the canonical RNase H site in the open conformation but was occluded in the closed conformation.

We solved the structure of human PRP8 RH mutants representing the V1788D PRP8 (yeast V1860D) and T1800E (yeast T1872E) first-step alleles; these revealed that both mutations introduce an additional hydrogen-bonding interaction within the closed conformation. Replacement of the Val1788 side chain with an aspartate results in the formation of a hydrogen bond to Tyr1786 at the base of the β-hairpin, whereas mutation of the β-branched side chain of Thr1800 to a glutamate allows sufficient freedom for the backbone peptide to rotate and also form a water-mediated hydrogen bond to Tyr1786 (**Fig. 3a**). These extra hydrogen bonds effectively anchor the β-strand in position, stabilizing the closed conformation.

We also determined the structures of two mutants I1790Y (yeast V1862Y) and T1789P (yeast T1861P) shown to be second-step suppressors on the basis of splicing of the ACT1-CUP1 reporters in yeast. We solved the 1.55-Å structure of the human I1790Y PRP8 RH mutant and observed the formation of a new hydrogen-bonding interaction between Tyr1790 and Asn1797 in the open conformation, in which the aromatic side chain of Tyr1790 spans the displaced loop (**Fig. 3b**). In the closed conformation, the side chains of Asn1797 and Tyr1790 project from opposite faces in the β-hairpin region. Therefore, the isoleucine-to-tyrosine mutation appears to stabilize the open conformation relative to the closed.

We crystallized and solved the 1.65-Å structure of the human T1789P mutant and the 1.95-Å structure of the T1789P R1865A double mutant (**Supplementary Note 3**). The T1789P mutation lies in the β-hairpin, and as expected this structure is disrupted in the closed conformation but with no discernible effect on the open conformation (**Fig. 3b**). We performed a crystallographic mixing experiment wherein equal concentrations of R1865A and the T1789P R1865A double mutant were mixed in the crystallization conditions

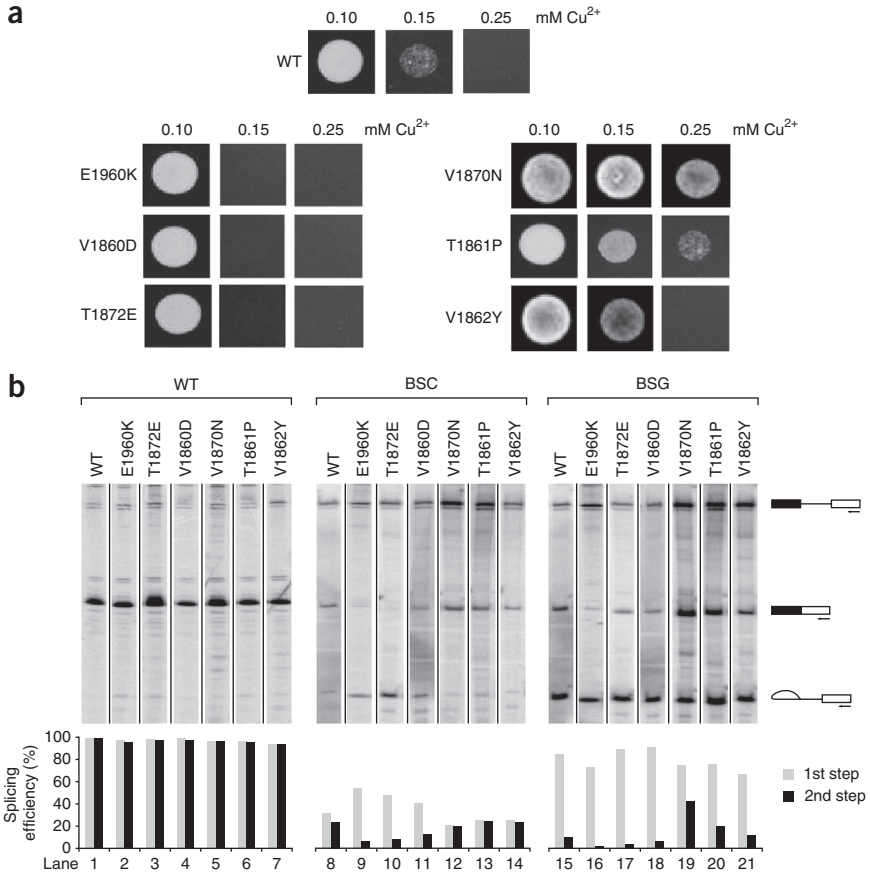

Figure 2 Characterization of *PRP8* RH-domain alleles. (**a**) Spot assays showing BSG ACT1-CUP1 reporter–dependent growth of yeast containing wild-type and mutant *PRP8* alleles in the presence of the indicated concentration of Cu^{2+}. (**b**) Denaturing PAGE analysis of reverse transcriptase primer extension with ^{32}P-labeled primer to examine steady-state splicing efficiencies in *PRP8* mutant yeast strains. Primer extension of ACT1-CUP1 RNA with wild-type, BSC or BSG sequences combined with *PRP8* alleles. Top, products corresponding to the mRNA, pre-mRNA and intron-lariat intermediate in the gel. Bottom, quantification of the first- and second-step efficiency. BSG, branch-site G; BSC, branch-site C; WT, wild type.

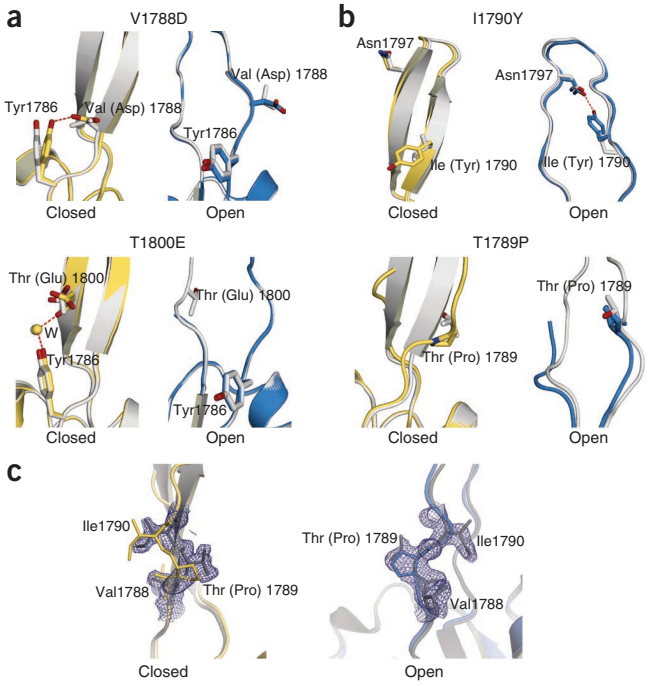

Figure 3 *PRP8* mutant alleles favor distinct conformations within the PRP8 RH domain. Shown are superpositions of X-ray structures of wild-type (gray) with mutant closed (yellow) or mutant open (cyan) conformers. (**a**) Top, detail showing formation of an additional hydrogen-bonding interaction to Tyr1786 in the closed conformation of the V1788D structure. Bottom, detail showing formation of a water (W)-mediated additional hydrogen-bonding interaction to Tyr1786 in the closed conformation of the T1800E structure. (**b**) Top, detail showing formation of a hydrogen bond across the loop with Asn1797 in the open conformation of the I1790Y structure. Bottom, detail showing disruption of the β-hairpin of the closed conformation in the T1789P structure. (**c**) X-ray structural analysis from a crystallographic mixing experiment with T1789P R1865A and R1865A proteins. Shown are models for structures of the R1865A (gray) and T1789P R1865A protein for the closed (yellow, left) and open (cyan, right) conformation. A $2F_o - F_c$ map contoured at 1σ, calculated from the data set of the T1789P R1865A–R1865A mixture crystal, is shown in dark blue.

(**Supplementary Note 3**). The 1.8-Å structure of the resulting crystal shows that only wild-type protein, which contains a threonine at position 1789, is visible in the β-hairpin closed conformation. In contrast, within the loop of the open conformation a mixture of threonine and proline is observed at this position (**Fig. 3c**). This suggests that the T1861P mutation favors the open conformation by destabilizing the closed conformation.

The results of these structural studies complement and rationalize the analysis of mutant *prp8* alleles in yeast. They suggest that two first-step alleles (V1860D and T1872E) result in the stabilization of the closed conformation of PRP8 RH and imply that this conformation is associated with the first step of splicing. The second-step allele V1862Y stabilizes the open conformation, whereas T1861P appears to destabilize the closed and thus favor the open conformation. The structure of the second-step allele L1798N (yeast V1870N) can also be modeled to suggest a hydrogen-bonding interaction stabilizing the open conformation (**Supplementary Note 4** and **Supplementary Fig. 3c**). These observations suggest that the open and metal-binding conformation of PRP8 RH is associated with the second step of splicing.

PRP8 metal binding is coupled to the second step of splicing

To examine the role of metal binding by PRP8 in the context of the spliceosome, we created a panel of five yeast mutants, modifying the identity of the inner-sphere ligand at position 1853 (**Fig. 4a**). These are all (with the exception of D1853E) predicted to impair, to varying degrees, magnesium coordination in the open conformation (**Supplementary Fig. 2b** and **Supplementary Note 5**). Moderate effects on growth were observed for a number of these mutants, although both D1853S and D1853N exhibited a strong temperature-sensitive phenotype at 37 °C. The D1853C mutant was impaired in growth at both 16 °C and 30 °C and did not grow at 37 °C. Mutation of Asp1853 to a hydrophobic residue (leucine or alanine), which would be incapable of either directly or indirectly coordinating Mg^{2+}, or to a positively charged residue (lysine) was lethal (**Supplementary Note 6**).

We prepared splicing extracts derived from all of the Asp1853 mutant strains and examined their splicing activity *in vitro* by using an *ACT1* pre-mRNA substrate (**Fig. 4b**). Overall, we observed a general trend wherein residues that should impair Mg^{2+}-ion binding impair splicing

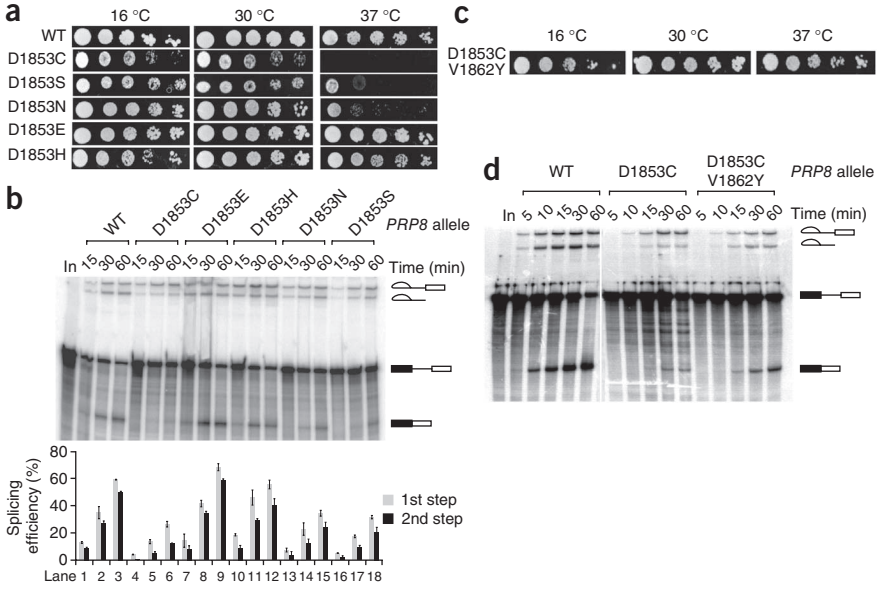

Figure 4 *PRP8* Asp1853 mutations selectively impair the second step of splicing. (**a**) Phenotypic analysis of *PRP8* Asp1853 mutations. Photographs show serial dilutions of cells from strains containing the indicated *PRP8* alleles, spotted onto YPD medium and incubated for 4 d at 16 °C, 2 d at 30 °C or 3 d at 37 °C. (**b**) Top, denaturing PAGE analysis of *in vitro* splicing of ^{32}P-labeled *ACT1* pre-mRNA in extracts prepared from strains containing the indicated Asp1853 *PRP8* mutants. The positions of the mRNA, pre-mRNA, intron-lariat and exon-lariat intermediate in the gel are indicated. Bottom, quantification of first- and second-step efficiencies. In, input. (**c**) D1853C rescue by the second-step allele V1862Y. Growth of a dilution series of the D1853C V1862Y yeast strain at 16 °C, 30 °C and 37 °C. (**d**) Denaturing PAGE analysis comparing *in vitro* splicing of ^{32}P-labeled actin pre-mRNA substrate in extracts prepared from wild-type, D1853C and D1853C V1862Y yeast strains. Error bars, s.d. from three independent experiments.

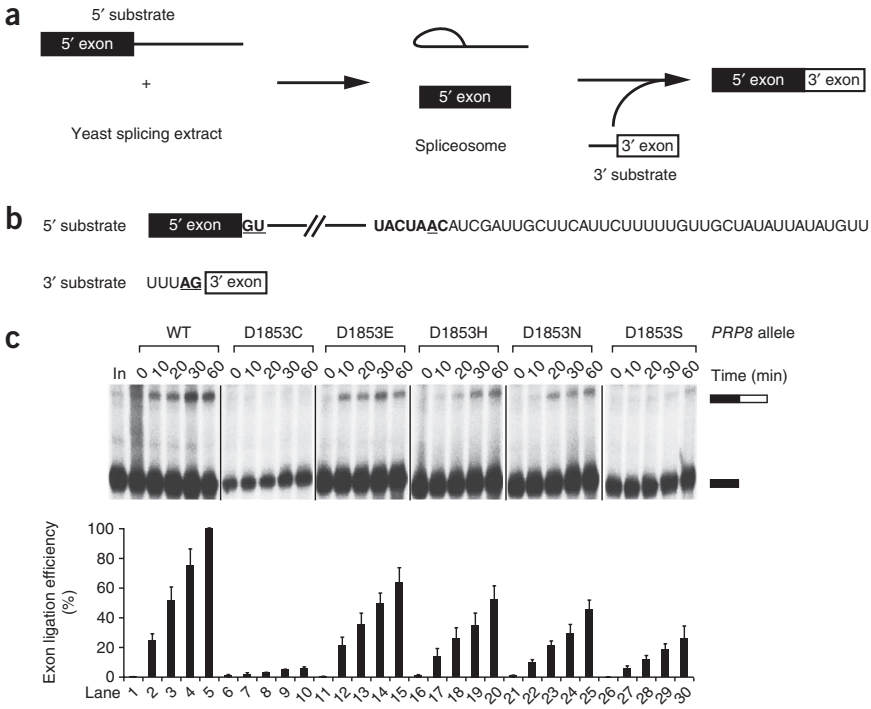

Figure 5 Bimolecular exon ligation assay implicates *PRP8* Asp1853 in the second transesterification step of pre-mRNA splicing. (**a**) Schematic representation of bimolecular exon ligation reaction. (**b**) RNA substrates used in the yeast bimolecular exon ligation. The 5′, 3′ splice site and the branch sequence are shown in bold. The 5′ GU dinucleotide, 3′ AG dinucleotide and branch adenosine are underlined. (**c**) Bimolecular exon ligation assay for analysis of the effect of Asp1853 mutations on the second step of splicing. Top, denaturing PAGE of products from a ^{32}P-labeled 5′ substrate RNA derived from ACT1 pre-mRNA, incubated under splicing conditions in wild-type and *PRP8* Asp1853 mutant yeast extracts and chased with unlabeled RNA containing the 3′ splice site (additional data in **Supplementary Fig. 5c**). The positions of the 5′ exon and ligated product are indicated. Bottom, quantification of exon ligation efficiency, corrected for the contribution from a degradation product present in the input lane and normalized to lane 5. Error bars, s.d. from three independent experiments.

substantially, with the second step more strongly affected than the first. We confirmed that mutation of Asp1853 results in a specific second-step defect by preparing extracts from pseudodiploid strains and specifically immunoprecipitating epitope-tagged mutant PRP8 containing spliceosomes from splicing reactions (**Supplementary Note 7** and **Supplementary Fig. 4a–c**). In all of these studies, the efficiency of the second step of splicing corresponds with the ability of an amino acid at position 1853 to coordinate or correctly position a Mg^{2+} ion at the canonical site (aspartate and glutamate > histidine; asparagine > serine >> cysteine).

Because D1853C was the most impaired viable mutant tested, we further examined the relationship of this mutation to the second-step conformation. We created a double mutant on the basis of the V1862Y second-step allele (D1853C V1862Y) and examined growth and splicing activity of extracts prepared from the mutant. Notably, V1862Y rescues the severe growth defect at 37 °C. Furthermore, as predicted for a second-step allele, V1862Y partially rescues the second-step splicing defect of D1853C in an *in vitro* assay with actin pre-mRNA (**Fig. 4c,d**).

One difficulty with mechanistic investigation of the second step of splicing is that a rate-determining conformational change may mask effects on the chemical step of splicing. An elegant approach to more directly observing the second step of splicing is the separation of the two steps in a bimolecular exon ligation reaction developed previously[22,23]. A pre-mRNA lacking a 3′ splice site undergoes the first but not the second step of splicing; subsequent addition of a 3′ splice site containing oligonucleotide in *trans* results in a bimolecular ligation that effectively separates the second chemical step from the first (**Fig. 5a**). This approach has been used successfully to investigate the effect, otherwise masked by a presumptive conformational change in the spliceosome, of substrate modifications on second-step splicing chemistry[24].

We established a bimolecular exon ligation reaction in yeast extracts to directly observe the effects of Asp1853 PRP8 mutants on the second step of splicing (**Fig. 5a**, **Supplementary Figs. 5** and **6** and **Supplementary Note 8**). We first synthesized a splicing substrate derived from the ACT1 pre-mRNA containing the 5′ exon, 5′ splice site, branch region and 40 downstream nucleotides (nt) but lacking a 3′ splice site. Additionally, we synthesized a 25-nt 3′ RNA substrate that included the last 5 nt of the intron (UUUAG) representing the 3′ splice site followed by 20 nt of 3′ exon sequence (**Fig. 5b**). Upon incubation of the 5′ substrate in wild-type extract, we observed an efficient first step of splicing but no second step. Chasing this reaction with the 3′ substrate resulted in bimolecular exon ligation. We then examined the splicing activity of extracts prepared from the panel of Asp1853 mutants by using this assay. All of these mutants carried out the first step of splicing with modest impairment corresponding to that observed for the full-length ACT1-substrate splicing assay (**Supplementary Fig. 5a,b**). An impairment of the exon ligation step matching the second-step defect observed with the full-length splicing substrate was also observed (**Fig. 5c** and **Supplementary Fig. 5c**). Notably, the efficiency of bimolecular exon ligation in extracts prepared from the D1853C mutant was ~3% of that observed in wild-type extract. This represents an order of magnitude further impairment with respect to the efficiency of exon ligation observed with the intact pre-mRNA. This observation suggests that the bimolecular exon ligation has revealed an effect of the D1853C mutation on a rate-limiting step and that this step involves the second transesterification reaction of splicing.

DISCUSSION

In the studies described here, we have observed crystallographically two distinct conformations of the PRP8 RH domain, one of which permits coordination of Mg^{2+} at a canonical and conserved metal-binding site (**Fig. 6a**). The structures of proteins corresponding to known suppressor alleles suggest both that the closed conformation of PRP8 corresponds to a first-step state and that the metal-binding open conformation corresponds to a second-step state. This is consistent with a model whereby PRP8 manifests conformations favoring or facilitating either the first or second transesterification steps of splicing (**Fig. 6b**).

There is a rich and complex provenance to the *prp8* suppressor alleles designated here and earlier[8,15] as first or second step. For example, the V1870N second-step allele was isolated as a suppressor of the branch-site A-to-G mutation, but it also acts as a suppressor of 5′- and 3′-splice-site mutations[8]. This is reminiscent of previous observations with respect to a number of other *prp8* suppressor alleles[25], which were interpreted to suggest a role for PRP8 at the catalytic core of the spliceosome. A number of *prp8* alleles relate to the transition from the U4–U6 snRNA base-pairing that precedes formation of the U2–U6

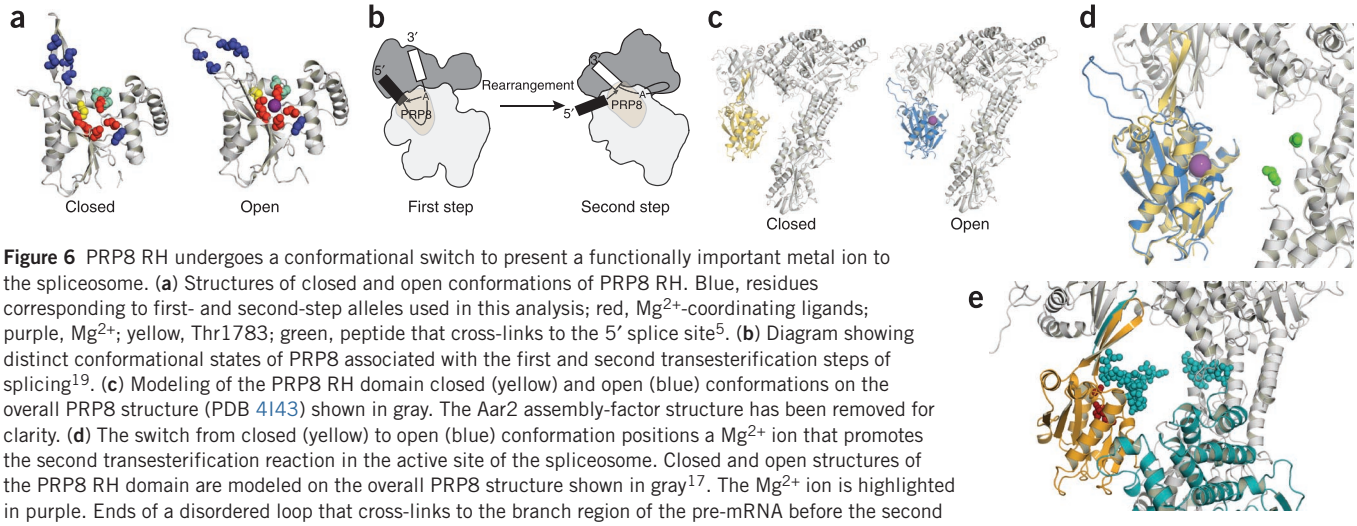

Figure 6 PRP8 RH undergoes a conformational switch to present a functionally important metal ion to the spliceosome. (**a**) Structures of closed and open conformations of PRP8 RH. Blue, residues corresponding to first- and second-step alleles used in this analysis; red, Mg^{2+}-coordinating ligands; purple, Mg^{2+}; yellow, Thr1783; green, peptide that cross-links to the 5′ splice site[5]. (**b**) Diagram showing distinct conformational states of PRP8 associated with the first and second transesterification steps of splicing[19]. (**c**) Modeling of the PRP8 RH domain closed (yellow) and open (blue) conformations on the overall PRP8 structure (PDB 4I43) shown in gray. The Aar2 assembly-factor structure has been removed for clarity. (**d**) The switch from closed (yellow) to open (blue) conformation positions a Mg^{2+} ion that promotes the second transesterification reaction in the active site of the spliceosome. Closed and open structures of the PRP8 RH domain are modeled on the overall PRP8 structure shown in gray[17]. The Mg^{2+} ion is highlighted in purple. Ends of a disordered loop that cross-links to the branch region of the pre-mRNA before the second step[17] are shown in green. (**e**) Aar2 sequesters the spliceosome active site cavity. The U5 snRNP assembly factor Aar2 (cyan) blocks the surface of the PRP8 RH domain (yellow), partially filling the active site cavity (aa 320–344, depicted as spheres) and stabilizes the PRP8 RH β-hairpin by extending the β-sheet[17] (aa 345–353). Mg^{2+}-coordinating residues in RH are shown in red.

structure within the mature spliceosome. In a screen for suppressors of the effects of hyperstabilization of the U4–U6 duplex, one study identified alleles of PRP8 containing V1860D, T1861P or V1862Y that were able to suppress this cold-sensitive (*cs*) defect[10]. It was noted in several studies that *prp8* alleles tend to suppress mutations either of the pre-mRNA splice sites or within spliceosomal components such as U4 snRNA[10,25,26]. Although some *prp8* alleles can suppress both types of defects, the general trend of segregation into two groups of *prp8* alleles in the context of the results reported here suggests that the PRP8 RH domain plays a part in earlier assembly-precatalytic steps within the spliceosome, which is distinct from the dynamics reported here. Beyond all of this is the identification of first- and second-step alleles outside of the PRP8 RH domain[8,11,12,19,27], which suggests a larger, concerted conformational change extending beyond that described for the PRP8 RH domain here.

The observation that PRP8 RH metal binding is only observed in the open conformation, combined with our structural and functional analyses of first- and second-step alleles, associates this state with the second step of splicing. Mutagenesis of the inner-sphere ligand Asp1853 combined with the effects of mutations at this site on splicing establish the importance of divalent-metal binding by PRP8 RH for the second transesterification step of splicing.

The recent structural analysis of a large fragment of yeast PRP8 in complex with the U5 snRNP–assembly factor Aar2 suggests the presence of a large cavity in PRP8, which on the basis of both mutational and cross-linking data has been proposed to encompass the active site of the spliceosome[5,6,12]. This cavity is large enough to contain the group II–intron active site RNA structure that has been proposed as a model for the U2–U6 snRNA components of the spliceosome active site[28]. The PRP8 RH domain, which also contains the PRP8 sequence that cross-links to the 5′ splice site, faces into this cavity directly across from a disordered loop that cross-links to the pre-mRNA branch region before the second step of splicing[17]. Thus, the conformational switch from closed to open conformations directly presents a metal ion, shown here to promote the second catalytic step of splicing, to the active site cavity of the spliceosome (**Fig. 6a–d**). These observations are consistent with a structural or catalytic role for the PRP8-bound metal ion in the spliceosomal active site for the second step of splicing and suggest that at this step the active site could contain both protein and RNA components. Notably, the C-terminal region of Aar2 lies across the PRP8 RH surface and stabilizes the β-hairpin structure by extending the β-sheet. This has the effect of blocking the cavity and locking the PRP8 RH domain in an assembly-precatalytic step conformation and is reminiscent of the sequestration of the U6 snRNA in the U4–U6 snRNA duplex that precedes formation of the catalytically active U2–U6 structure and precludes metal binding by U6 snRNA[29,30] (**Fig. 6e**).

The precise role of the bound metal ion within the open conformation of the PRP8 RH domain remains to be determined and will require further structural and functional analysis. This metal could perform a structural role with respect to stabilizing the second-step conformation of this domain, it could have a role in positioning or stabilizing either substrate or active site snRNA components, or it could have a direct role in catalysis of the second step.

It has long been believed that the spliceosome is in essence a ribozyme, in part on the basis of the mechanistic similarity between self-splicing group II introns and the processing of nuclear pre-mRNAs[31]. There is also considerable evidence for the role of the spliceosomal U2–U6 snRNA structure, particularly U6 snRNA, in catalysis of both steps of splicing[29,30,32]. High-resolution structural analyses of the group I and group II introns have supported a general two-metal-ion mechanism that was proposed for these catalytic RNAs as well as the spliceosome, on the basis of analysis of phosphoryl transfer by protein enzymes[28,33,34]. There is nevertheless scope for the involvement of more or fewer metal ions in similar enzymatic transformations. A recent study has proposed a mechanism for type II and IA topoisomerases wherein the transition state is stabilized by a single bound metal and conserved arginine[35]. A detailed characterization of the mechanism of DNA polymerase η persuasively suggests the participation of a third metal ion in the stabilization of an intermediate state[36], and three active site metals have been observed in the structures of other enzymes involved in the catalysis of phosphoryl transfer[37–40]. There is also compelling functional evidence for the participation of three metal ions at the active site of the group I intron[41]. Thus there is the potential for PRP8 to participate as part of a three-metal spliceosomal active site that would include two metals bound by an snRNA catalytic structure evolutionarily derived from a group II–like intron active site and a third contributed by the protein[17,33,34].

The conformational change described here represents a specific switch mechanism between the two steps of splicing. Further, that this switch is coupled to the binding of a functionally important metal ion implicates it as a key regulatory mechanism in promotion of the second chemical step of splicing.

METHODS

Methods and any associated references are available in the online version of the paper.

Accession codes. Coordinates and structure factors for the PRP8 RH domain X-ray structures have been deposited in the Protein Data Bank under accession codes 4JK7, 4JK8, 4JK9, 4JKA, 4JKB, 4JKC, 4JKD, 4JKE, 4JKF, 4JKG and 4JKH.

Note: Supplementary information is available in the online version of the paper.

ACKNOWLEDGMENTS

This work was supported by an Operating grant to A.M.M. from the Canadian Institutes of Health Research (CIHR) and a US National Institutes of Health grant to J.P.S. and J. Piccirilli (R01GM088656). We would like to thank M. Friis and M. Schultz for helpful advice, J. Beggs (University of Edinburgh, Edinburgh, UK) and C. Guthrie (University of California, San Francisco, San Francisco, California, USA) for providing yeast strains and plasmids and D. Brow (University of Wisconsin–Madison, Madison, Wisconsin, USA) for providing the PRP8 V1862Y plasmid. Research described in this paper was performed at the Advanced Light Source (Berkeley, California, USA; supported by the US Department of Energy under contract no. DE-AC02-05CH11231) and the Canadian Light Source (supported by the Natural Sciences and Engineering Research Council of Canada, the National Research Council Canada, CIHR, the Province of Saskatchewan, Western Economic Diversification Canada and the University of Saskatchewan).

AUTHOR CONTRIBUTIONS

M.J.S., T.W., D.B.R. and A.M.M. designed the study; M.J.S. created mutant yeast strains, crystallized protein, collected X-ray diffraction data, solved the structures and performed *in vivo* and *in vitro* assays including development of the bimolecular exon ligation; T.W. created mutant PRP8 yeast strains, crystallized protein, collected X-ray diffraction data and carried out *in vivo* and *in vitro* assays; K.A.A. purified and crystallized proteins; S.F. and J.P.S. independently designed and tested mutants and critically analyzed data; D.B.R. designed, crystallized and analyzed mutants; P.L. provided technical expertise and helped design experiments in yeast; M.J.S., T.W. and A.M.M. wrote the manuscript.

COMPETING FINANCIAL INTERESTS

The authors declare no competing financial interests.

1. Jurica, M.S. & Moore, M.J. Pre-mRNA splicing: awash in a sea of proteins. *Mol. Cell* **12**, 5–14 (2003).
2. Rappsilber, J., Ryder, U., Lamond, A.I. & Mann, M. Large-scale proteomic analysis of the human spliceosome. *Genome Res.* **12**, 1231–1245 (2002).
3. Zhou, Z., Licklider, L.J., Gygi, S.P. & Reed, R. Comprehensive proteomic analysis of the human spliceosome. *Nature* **419**, 182–185 (2002).
4. Madhani, H.D. & Guthrie, C. A novel base-pairing interaction between U2 and U6 snRNAs suggests a mechanism for the catalytic activation of the spliceosome. *Cell* **71**, 803–817 (1992).
5. Reyes, J.L., Gustafson, E.H., Luo, H.R., Moore, M.J. & Konarska, M.M. The C-terminal region of hPrp8 interacts with the conserved GU dinucleotide at the 5′ splice site. *RNA* **5**, 167–179 (1999).
6. Turner, I.A., Norman, C.M., Churcher, M.J. & Newman, A.J. Dissection of Prp8 protein defines multiple interactions with crucial RNA sequences in the catalytic core of the spliceosome. *RNA* **12**, 375–386 (2006).
7. Vidal, V.P., Verdone, L., Mayes, A.E. & Beggs, J.D. Characterization of U6 snRNA-protein interactions. *RNA* **5**, 1470–1481 (1999).
8. Liu, L., Query, C.C. & Konarska, M.M. Opposing classes of prp8 alleles modulate the transition between the catalytic steps of pre-mRNA splicing. *Nat. Struct. Mol. Biol.* **14**, 519–526 (2007).
9. Kuhn, A.N., Reichl, E.M. & Brow, D.A. Distinct domains of splicing factor Prp8 mediate different aspects of spliceosome activation. *Proc. Natl. Acad. Sci. USA* **99**, 9145–9149 (2002).
10. Kuhn, A.N. & Brow, D.A. Suppressors of a cold-sensitive mutation in yeast U4 RNA define five domains in the splicing factor Prp8 that influence spliceosome activation. *Genetics* **155**, 1667–1682 (2000).
11. Umen, J.G. & Guthrie, C. Mutagenesis of the yeast gene *PRP8* reveals domains governing the specificity and fidelity of 3′ splice site selection. *Genetics* **143**, 723–739 (1996).
12. Grainger, R.J. & Beggs, J.D. Prp8 protein: at the heart of the spliceosome. *RNA* **11**, 533–557 (2005).
13. Abelson, J. Is the spliceosome a ribonucleoprotein enzyme? *Nat. Struct. Mol. Biol.* **15**, 1235–1237 (2008).
14. Ritchie, D.B. *et al.* Structural elucidation of a PRP8 core domain from the heart of the spliceosome. *Nat. Struct. Mol. Biol.* **15**, 1199–1205 (2008).
15. Yang, K., Zhang, L., Xu, T., Heroux, A. & Zhao, R. Crystal structure of the β-finger domain of Prp8 reveals analogy to ribosomal proteins. *Proc. Natl. Acad. Sci. USA* **105**, 13817–13822 (2008).
16. Pena, V., Rozov, A., Fabrizio, P., Luhrmann, R. & Wahl, M.C. Structure and function of an RNase H domain at the heart of the spliceosome. *EMBO J.* **27**, 2929–2940 (2008).
17. Galej, W.P., Oubridge, C., Newman, A.J. & Nagai, K. Crystal structure of Prp8 reveals active site cavity of the spliceosome. *Nature* **493**, 638–643 (2013).
18. Nowotny, M., Gaidamakov, S.A., Crouch, R.J. & Yang, W. Crystal structures of RNase H bound to an RNA/DNA hybrid: substrate specificity and metal-dependent catalysis. *Cell* **121**, 1005–1016 (2005).
19. Query, C.C. & Konarska, M.M. Suppression of multiple substrate mutations by spliceosomal *prp8* alleles suggests functional correlations with ribosomal ambiguity mutants. *Mol. Cell* **14**, 343–354 (2004).
20. Fouser, L.A. & Friesen, J.D. Mutations in a yeast intron demonstrate the importance of specific conserved nucleotides for the two stages of nuclear mRNA splicing. *Cell* **45**, 81–93 (1986).
21. Vijayraghavan, U. *et al.* Mutations in conserved intron sequences affect multiple steps in the yeast splicing pathway, particularly assembly of the spliceosome. *EMBO J.* **5**, 1683–1695 (1986).
22. Anderson, K. & Moore, M.J. Bimolecular exon ligation by the human spliceosome. *Science* **276**, 1712–1716 (1997).
23. Anderson, K. & Moore, M.J. Bimolecular exon ligation by the human spliceosome bypasses early 3′ splice site AG recognition and requires NTP hydrolysis. *RNA* **6**, 16–25 (2000).
24. Gordon, P.M., Sontheimer, E.J. & Piccirilli, J.A. Metal ion catalysis during the exon-ligation step of nuclear pre-mRNA splicing: extending the parallels between the spliceosome and group II introns. *RNA* **6**, 199–205 (2000).
25. Collins, C.A. & Guthrie, C. Allele-specific genetic interactions between Prp8 and RNA active site residues suggest a function for Prp8 at the catalytic core of the spliceosome. *Genes Dev.* **13**, 1970–1982 (1999).
26. Kuhn, A.N., Li, Z. & Brow, D.A. Splicing factor Prp8 governs U4/U6 RNA unwinding during activation of the spliceosome. *Mol. Cell* **3**, 65–75 (1999).
27. Siatecka, M., Reyes, J.L. & Konarska, M.M. Functional interactions of Prp8 with both splice sites at the spliceosomal catalytic center. *Genes Dev.* **13**, 1983–1993 (1999).
28. Adams, P.L., Stahley, M.R., Kosek, A.B., Wang, J. & Strobel, S.A. Crystal structure of a self-splicing group I intron with both exons. *Nature* **430**, 45–50 (2004).
29. Yean, S.L., Wuenschell, G., Termini, J. & Lin, R.J. Metal-ion coordination by U6 small nuclear RNA contributes to catalysis in the spliceosome. *Nature* **408**, 881–884 (2000).
30. Koodathingal, P., Novak, T., Piccirilli, J.A. & Staley, J.P. The DEAH box ATPases Prp16 and Prp43 cooperate to proofread 5′ splice site cleavage during pre-mRNA splicing. *Mol. Cell* **39**, 385–395 (2010).
31. Sontheimer, E.J., Sun, S. & Piccirilli, J.A. Metal ion catalysis during splicing of premessenger RNA. *Nature* **388**, 801–805 (1997).
32. Sashital, D.G., Cornilescu, G., McManus, C.J., Brow, D.A. & Butcher, S.E. U2–U6 RNA folding reveals a group II intron-like domain and a four-helix junction. *Nat. Struct. Mol. Biol.* **11**, 1237–1242 (2004).
33. Toor, N., Keating, K.S., Taylor, S.D. & Pyle, A.M. Crystal structure of a self-spliced group II intron. *Science* **320**, 77–82 (2008).
34. Steitz, T.A. & Steitz, J.A. A general two-metal-ion mechanism for catalytic RNA. *Proc. Natl. Acad. Sci. USA* **90**, 6498–6502 (1993).
35. Schmidt, B.H., Burgin, A.B., Deweese, J.E., Osheroff, N. & Berger, J.M. A novel and unified two-metal mechanism for DNA cleavage by type II and IA topoisomerases. *Nature* **465**, 641–644 (2010).
36. Nakamura, T., Zhao, Y., Yamagata, Y., Hua, Y.J. & Yang, W. Watching DNA polymerase η make a phosphodiester bond. *Nature* **487**, 196–201 (2012).
37. Le Du, M.H. *et al.* Artificial evolution of an enzyme active site: structural studies of three highly active mutants of *Escherichia coli* alkaline phosphatase. *J. Mol. Biol.* **316**, 941–953 (2002).
38. Kim, E.E. & Wyckoff, H.W. Reaction mechanism of alkaline phosphatase based on crystal structures: two-metal ion catalysis. *J. Mol. Biol.* **218**, 449–464 (1991).
39. Romier, C., Dominguez, R., Lahm, A., Dahl, O. & Suck, D. Recognition of single-stranded DNA by nuclease P1: high resolution crystal structures of complexes with substrate analogs. *Proteins* **32**, 414–424 (1998).
40. Garcin, E.D. *et al.* DNA apurinic-apyrimidinic site binding and excision by endonuclease IV. *Nat. Struct. Mol. Biol.* **15**, 515–522 (2008).
41. Shan, S., Yoshida, A., Sun, S., Piccirilli, J.A. & Herschlag, D. Three metal ions at the active site of the *Tetrahymena* group I ribozyme. *Proc. Natl. Acad. Sci. USA* **96**, 12299–12304 (1999).

ONLINE METHODS

Protein expression, purification and crystallization. hPRP8$_{1769–1990}$ protein was grown and purified as previously described[14]; crystals were grown at 23 °C by using the hanging-drop vapor-diffusion technique. Crystals of native protein were grown by mixing 1 µl of 10 mg ml^{-1} protein solution (10 mM Tris, pH 8.0, 0.1 mM EDTA, 5 mM DTT and 0.02% NaN_3) with 1 µl of precipitant (2.5 M NaCl, 100 mM Tris, pH 7.0 and 200 mM $MgCl_2$ or 10–14% (w/v) PEG 4000, 100 mM Tris, pH 7.5, and 300 mM $MgCl_2$). Crystals were transferred into cryoprotectant (25% (w/v) PEG 4000, 16% (v/v) glycerol and 100 mM Tris, pH 7.5) with the indicated concentration of divalent metal as a chloride salt and frozen in liquid nitrogen for data collection[14].

Wild-type and mutant PRP16, PRP22 and PRP43 proteins were grown and purified as previously described[42,43].

Data collection and processing. Data were collected at beamline 8.3.1 of the Advanced Light Source, Lawrence Berkeley National Laboratory, at beamline CMCF-1 at the Canadian Light Source, University of Saskatchewan, Saskatoon, and on an *R*-axis rotating Cu-anode X-ray source. For the wild-type and R1865A PRP8 RH crystals grown in 300 mM $MgCl_2$, a single-wavelength experiment was performed at 0.97949 Å at a temperature of 105 K. Data were processed and scaled by using HKL[44]; Friedel pairs were not merged when anomalous scattering maps were required. Anomalous scattering maps were calculated by using the CCP4 suite[45].

Model building and refinement. The structures were solved by molecular replacement by using Refmac[46] to refine, with PDB 3ENB as a starting model. Water molecules were built by using ARP/wARP[47]. Iterative cycles of refinement in Refmac against the merged data set and manual model building in Coot were used to complete and refine the models[48]. Ramachandran statistics for the final refined models of wild type and R1865A are: wild type grown in 300 mM $MgCl_2$, 98.4% favored, 0.0% outliers; R1865A grown in 300 mM $MgCl_2$, 98.2% favored, 0.0% outliers. All additional Ramachandran statistics are given in **Supplementary Table 1**.

Creation of mutant *S. cerevisiae* strains and splicing extracts. Mutant *prp8* genes were created by gap repair of plasmid pJU186 (ref. 49) containing a *HIS3* -selectable marker and PRP8 gene. Mutant plasmids were transformed into strain JDY8.06 (*ura3-52*, *leu2-3,-112, ade2*, *his3-A1*, *trpl-289*, *prp8::LEU2*, *pJU169* (*PRP8*, *URA3*, *CEN*, *ARS*); gift from J. Beggs, University of Edinburgh, UK) containing wild-type PRP8 on a counterselectable *URA3*-marked plasmid[50]. After transformation with pJU186, cells were selected by growth at 30 °C on SDC plates lacking histidine and leucine. Transformants were streaked on medium lacking histidine and leucine and containing 5-fluoroorotic acid (5-FOA) to select for cells lacking the *URA3* plasmid[51]. Cells from a single colony that survived on 5-FOA plates were grown in medium lacking histidine, and total DNA was extracted by using a DNeasy kit (Qiagen). All mutant PRP8 strains were verified by sequencing. Splicing extracts were prepared as described elsewhere[49].

For creation of copper-resistant strains, the ACT1-CUP1 plasmid containing the wild-type sequence, BSC or BSG mutations was co-transformed along with pJU186 containing wild-type or mutant PRP8 into yJU75 (ref. 11) (*MATa*, *ade2 cup1D::ura3 his3 leu2 lys2 prp8D::LYS2 trp1*, *pJU169* (*PRP8 URA3 CEN ARS*)). Transformants were streaked on medium lacking histidine and leucine and containing 5-FOA to select for cells lacking the *URA3* plasmid. Cells surviving on 5-FOA plates were grown in medium lacking histidine, and total DNA was extracted by using a DNeasy kit (Qiagen). All mutant PRP8 strains were verified by sequencing.

For the creation of pseudodiploid strains, PRP8 was knocked out with a *LEU2*-marked fragment in yJPS662, the knockout confirmed by PCR and viability rescued with PRP8 on *URA3*-marked plasmid generating yJPS1481. To obtain pseudodiploid strains, yJPS1481 was transformed with wild-type or mutant PRP8 on a *HIS3* plasmid, and transformants that retained both the wild-type *URA3* and the *HIS3* PRP8 plasmids were selected on uracil-histidine dropout medium. Mutant PRP8 plasmids were generated from the wild-type plasmid pJU204 (PRP8-HA, HIS3, gift from C. Guthrie) by QuikChange PCR (Agilent) and verified by sequencing.

Growth assays. For spot-test analysis, yeast strains were inoculated in YPD medium (1% yeast extract, 2% peptone and 2% dextrose) and grown overnight at 30 °C with shaking. The next day, the OD at 600 nm was determined, and 10-µl serial dilutions from 1×10^6 to 1.6×10^3 cells ml^{-1} were spotted onto YPD plates. Plates were photographed after 2 d at 30 °C, 3 d at 37 °C and 4 d at 16 °C.

For the copper growth assay, cultures containing the BSG ACT1-CUP1 and PRP8 mutant plasmids were grown overnight in SDC-leucine-histidine medium, diluted to $A_{600} = 0.2$ and spotted onto SDC-leucine-histidine agar plates containing the indicated concentrations of $CuSO_4$ (ref. 52). Plates were photographed after 3 d at 30 °C.

Primer extension. RNA was extracted by using hot phenol[53]. Cultures containing the ACT1-CUP1 and PRP8 mutant plasmids were grown overnight in SDC-leucine-histidine medium, diluted to 5 ml ($A_{600} = 0.2$) and then grown in SDC-leucine-histidine medium for an additional 6 h to $A_{600} = 1.0$. The cells were spun down and resuspended in 400 µl of AE buffer with 10% SDS (50 mM NaOAc and 10 mM EDTA, pH 5.0). Hot phenol/AE solution (400 µl) was immediately added and incubated at 65 °C for 30 min. After centrifugation at 21,000*g*, the upper phase was transferred into clean tubes, and the hot phenol/AE treatment was repeated. The upper phase was extracted three or four times with phenol/chloroform/isoamyl alcohol and chloroform followed by ethanol precipitation. The pellet was resuspended in 10 µl ddH_2O.

Primer extensions were carried out by using the YAC6 primer complementary to exon 2 of ACT1 (ref. 54). The primer was end-labeled with [γ-^{32}P]ATP (3,000 Ci/mmol, PerkinElmer). Primer extensions were performed by using the RevertAid H minus First Strand cDNA Synthesis Kit (Fermentas). First, 12 µl of the mixture (1 µg total RNA and 2 pmol labeled primer) was heated to 70 °C for 10 min and slowly cooled down to 40 °C. The reaction was chilled on ice, supplemented to 20 µl (4 µl reaction buffer, 1 U RNase inhibitor, 1 mM dNTP mix and 10 U reverse transcriptase), then incubated for 5 min at 37 °C and 55 min at 42 °C. The reaction was terminated, and the RNA was degraded with 0.5 M NaOH at 70 °C. Extension products were extracted with phenol/chloroform/isoamyl alcohol and chloroform, then ethanol-precipitated. The pellet was resuspended, separated in gels containing 7% polyacrylamide and 8 M urea and visualized by autoradiography.

Construction of RNA substrates. The ACT1 and UBC4 pre-mRNAs were made by *in vitro* transcription with T7 RNA polymerase and [α-^{32}P]ATP by using a PCR template amplified from the appropriate plasmid. The 25-µl reaction (40 mM Tris, pH 8.0, 6 mM $MgCl_2$, 10 mM NaCl, 2 mM spermidine, 0.5 mM CTP, 0.5 mM GTP, 0.5 mM UTP, 60 µM ATP, 1.32 µM [α-^{32}P]ATP (PerkinElmer), 5 ng DNA template, 10 mM DTT and 1 µl T7 RNA polymerase) was incubated at 37 °C for 4 h. The reaction was then separated on a PAGE gel containing 7% 19:1 acrylamide/bisacrylamide and 8 M urea.

The 5′ ACT1 substrate used in the exon ligation assay was synthesized by *in vitro* transcription to yield the following sequence: 5′-CUUUUAGAUUUU UCACGCUUACUGCUUUUUUCUUCCCAAGAUCGAAAAUUUACUGA AUUAACAAUGGAUUCUGGUAUGUUCUAGCGCUUGCACCAUCCCA UUUAACUGUAAGAAGAAUUGCACGGUCCCAAUUGCUCGAGAGAUU UCUCUUUUACCUUUUUUUACUAUUUUUCACUCUCCCAUAACCUCCU AUAUUGACUGAUCUGUAAUAACCACGAUAUUAUUGGAAUAAAUAGGG GCUUGAAAUUUGGAAAAAAAAAAAAACUGAAAUAUUUUCGUGAUA AGUGAUAGUGAUAUUCUUCUUUUAUUUGCUACUGUGUCUCAUGUAC UAACAUCGAUUGCUUCAUUCUUUUUGUUGCUAUAUUAUAUGUU-3′.

The 3′ ACT1 substrate used in the exon ligation assay was synthesized (IDT) with the following sequence: 5′-UUUAGAGGUUGCUGCUUUGGUUAUU-3′.

Splicing assays. Splicing reactions (10 µl) were performed as described[54] in reactions containing 2 mM ATP, 2.5 mM $MgCl_2$, 3% (w/v) PEG 8000, 60 mM potassium phosphate, pH 7.0, 20 mM KCl, 8 mM HEPES, 8% (v/v) glycerol, 80 µM EDTA, 0.2 mM DTT and 1 nM pre-mRNA. Reactions were quenched with 10 µl of stop solution (1 mg ml^{-1} proteinase K, 50 mM EDTA and 1% SDS) and then incubated at 65 °C for 15 min. Each sample was extracted with phenol/chloroform/isoamyl alcohol, then chloroform, and was then ethanol-precipitated. Pellets were resuspended in loading dye, separated on PAGE gels containing 7% 19:1 acrylamide/bisacrylamide and 8 M urea, exposed to a phosphor storage screen and scanned with a PhosphorImager (Molecular Dynamics).

For the assay of extracts from pseudodiploid strains, UBC4 pre-mRNA was preincubated for 20 min in 60-µl reactions. Mutant PRP43 protein was added

to block release of the excised intron and to allow accurate quantification of all splicing species associated with the HA-tagged PRP8. Intermediates associated with PRP8-HA were immunoprecipitated with anti-HA antibody conjugated to protein A–Sepharose (Sigma) (25 µl slurry in IPP150 (10 mM Tris-HCl, pH 8, 150 mM NaCl and 0.01% NP-40 substitute (Fluka))). Beads were incubated with the splicing reactions for 90 min at 4 °C and washed three times with ten volume equivalents of IPP150. RNA was extracted with phenol/chloroform/isoamyl alcohol and separated by 15% denaturing PAGE.

For the exon ligation assay, the labeled 5′ portion of the ACT1 pre-mRNA was preincubated for 30 min in 10-µl splicing reactions. Exon ligation was initiated by addition of the 3′ portion of the ACT1 RNA substrate to splicing reactions, and incubation then continued for 10, 20, 30 and 60 min. The exon ligation product was amplified by RT-PCR, and its identity was confirmed by sequencing. Quantifications were performed by using ImageQuant (Molecular Dynamics).

42. Tanaka, N. & Schwer, B. Mutations in *PRP43* that uncouple RNA-dependent NTPase activity and pre-mRNA splicing function. *Biochemistry* **45**, 6510–6521 (2006).
43. Mayas, R.M., Maita, H., Semlow, D.R. & Staley, J.P. Spliceosome discards intermediates via the DEAH box ATPase Prp43p. *Proc. Natl. Acad. Sci. USA* **107**, 10020–10025 (2010).
44. Otwinowski, Z.M. & Minor, W. Processing of X-ray diffraction data collected in oscillation mode. *Methods Enzymol.* **276**, 307–326 (1997).
45. Potterton, E., Briggs, P., Turkenburg, M. & Dodson, E. A graphical user interface to the CCP4 program suite. *Acta Crystallogr. D Biol. Crystallogr.* **59**, 1131–1137 (2003).
46. Murshudov, G.N., Vagin, A.A. & Dodson, E.J. Refinement of macromolecular structures by the maximum-likelihood method. *Acta Crystallogr. D Biol. Crystallogr.* **53**, 240–255 (1997).
47. Terwilliger, T.C. Automated main-chain model building by template matching and iterative fragment extension. *Acta Crystallogr. D Biol. Crystallogr.* **59**, 38–44 (2003).
48. Emsley, P. & Cowtan, K. Coot: model-building tools for molecular graphics. *Acta Crystallogr. D Biol. Crystallogr.* **60**, 2126–2132 (2004).
49. Umen, J.G. & Guthrie, C. A novel role for a U5 snRNP protein in 3′ splice site selection. *Genes Dev.* **9**, 855–868 (1995).
50. Brown, J.D. & Beggs, J.D. Roles of PRP8 protein in the assembly of splicing complexes. *EMBO J.* **11**, 3721–3729 (1992).
51. Boeke, J.D., Trueheart, J., Natsoulis, G. & Fink, G.R. 5-Fluoroorotic acid as a selective agent in yeast molecular genetics. *Methods Enzymol.* **154**, 164–175 (1987).
52. Lesser, C.F. & Guthrie, C. Mutational analysis of pre-mRNA splicing in *Saccharomyces cerevisiae* using a sensitive new reporter gene, CUP1. *Genetics* **133**, 851–863 (1993).
53. Köhrer, K. & Domdey, H. Preparation of high molecular weight RNA. *Methods Enzymol.* **194**, 398–405 (1991).
54. Lin, R.J., Newman, A.J., Cheng, S.C. & Abelson, J. Yeast mRNA splicing *in vitro*. *J. Biol. Chem.* **260**, 14780–14792 (1985).

doi:10.1038/nsmb.2556